

AUIQ Complementary Biological System

ISSN: 3007-973X Journal homepage: https://acbs.alayen.edu.iq



Manuscript 1035

Biosorption of Crystal Violet onto Fenugreek Seed Powder: Comprehensive Optimization Through Response Surface Methodology and Elucidation of Dye Uptake Mechanism

Hasan M. Agha

Zaher Mundher Yaseen

Wafaa Raji Alfatlawi

Khansaa Al-Essa

Abdallah Reghioua

Hussein A. Kazem

Lee D. Wilson

Follow this and additional works at: https://acbs.alayen.edu.iq/journal



Part of the Biology Commons, Biotechnology Commons, and the Medicine and Health Sciences Commons



Scan the QR to view the full-text article on the journal website



ORIGINAL STUDY

Biosorption of Crystal Violet onto Fenugreek Seed Powder: Comprehensive Optimization Through Response Surface Methodology and Elucidation of Dye Uptake Mechanism

Hasan M. Agha[®] a,*, Zaher Mundher Yaseen b, Wafaa Raji Alfatlawi c, Khansaa Al-Essa d, Abdallah Reghioua e,f, Hussein A. Kazem g, Lee D. Wilson h

- ^a Faculty of Applied Sciences, Universiti Teknologi MARA, 40450 Shah Alam, Selangor, Malaysia
- ^b Civil and Environmental Engineering Department, King Fahd University of Petroleum & Minerals, Dhahran 31261, Saudi Arabia
- ^c Applied Chemistry Department, College of Applied Science, University of Technology, Iraq
- ^d Department of Chemistry, Jerash University, Jerash 26150, Jordan
- ^e Fac. Technology, University of El Oued, 39000 El Oued, Algeria
- f Laboratory of Applied Chemistry and Environment, University of El Oued, 39000 El Oued, Algeria
- g Faculty of Engineering, Sohar University, PO Box 44, PCI 311, Sohar, Oman
- ^h Department of Chemistry, University of Saskatchewan, Saskatoon, SK. S7N 5C9, Canada

ABSTRACT

This work investigates the efficacy of fenugreek seed powder (FSP), an agricultural product, as an economical and sustainable biosorbent for the extraction of crystal violet (CV) dye from aqueous environments. The biosorbent was analyzed using XRD, FTIR, and SEM-EDX, validating its amorphous structure, surface functional groups, and porous shape. Batch biosorption tests were adjusted utilizing a Box–Behnken design (BBD), incorporating three independent variables: FSP dose (0.02–0.1 g/100 mL), pH (4–10), and time (5–60 min). The model exhibited exceptional prediction accuracy ($R^2=0.99$, CV = 2.12%) and recognized all three variables as statistically significant (p < 0.05). The maximum CV removal attained was 91.8% efficiency at an FSP dose of 0.1 g/100 mL, pH 7, and a time of 60 minutes. FTIR examination indicated changes in the –OH, C=O, and C–O functional groups, signifying their participation in dye interaction, whilst SEM pictures validated dye deposition on the biosorbent surface. The biosorption process was ascribed to electrostatic forces, hydrogen bonding, π – π stacking, and pore filling. These findings underscore FSP as a viable, economical biosorbent for the removal of cationic dyes in wastewater treatment applications.

Keywords: Biosorption mechanism, Box–Behnken design, Cationic dye remediation, Response surface methodology, Sustainable biosorbent, Wastewater treatment

1. Introduction

Synthetic dyes constitute a major category of environmental pollutants, mostly due to the substantial release of dye-contaminated effluents from the textile, leather, and paper industries [1, 2]. The textile industry accounts for roughly 60–70% of worldwide

dye wastewater discharge, rendering it the primary source of dye pollution in aquatic ecosystems [3]. Crystal violet (CV), a cationic triphenylmethane dye, has garnered significant attention among contaminants owing to its remarkable durability, vivid hue, and possible detrimental effects on ecosystems and human health [4, 5]. CV is extensively employed

Received 7 August 2025; revised 11 August 2025; accepted 14 August 2025. Available online 26 August 2025

Corresponding author.

E-mail address: hasanagha586@gmail.com (H. M. Agha).

in textile production, biological staining, and the paper sector; nonetheless, its refractory properties and resistance to biodegradation render it a lasting environmental threat [6, 7]. The unregulated discharge of CV-contaminated wastewater results in less light penetration in aquatic ecosystems, oxygen depletion, and bioaccumulation, presenting hazards including mutagenicity, carcinogenicity, and cytotoxicity to both aquatic creatures and humans [8, 9]. Reported concentrations of CV in untreated textile effluents can reach 5-100 mg/L, while levels up to 20 mg/L have been detected in surface waters near dye-manufacturing facilities [10]. Prolonged exposure to such concentrations poses serious ecological risks and long-term health hazards, underscoring the urgent need for effective and sustainable removal strategies [11].

In order to alleviate the environmental impact of CV and other synthetic dyes, a variety of physicochemical and biological remediation strategies have been investigated, such as adsorption [12, 13], membrane filtration [14], advanced oxidation [15], and coagulation-flocculation [16]. Adsorption has become a widely recognized method for dye removal due to its simplicity, efficiency, and economic feasibility, particularly when biosorbents derived from agricultural waste are used [17]. Biosorption is acknowledged as a very feasible and successful technique that offers several advantages, such as cost efficiency, operational simplicity, environmental sustainability, limited secondary waste production, and superior pollutant removal efficacy [18]. This method employs biological matrices as sorbents, which facilitate the rapid and reversible binding of ions or pigment molecules from aqueous media to the surface functional groups of the biosorbent [19]. The biosorption potential of a diverse array of biomaterials, such as biopolymers, bacteria, algae, and agricultural debris, has been the subject of extensive research. This is due to the abundance of functional groups that are capable of effectively interacting with both ionic and non-ionic pollutants [20]. Considering these attributes, several biomass feedstocks, such as Olea europaea stones [21], xanthan gum [22], Macadamia integrifoli shell [23], sugarcane bagasse [24], Parkia speciosa Hassk peel [25], and Cynara scolymus [26], have been effectively utilized for pollutant removal. Fenugreek (Trigonella foenum-graecum L.) seeds produce a significant quantity of solid waste as a by-product of agricultural and industrial processing [27, 28]. This residue has a naturally porous structure, rendering it a viable low-cost biosorbent for environmental applications [29]. Due to these properties, fenugreek seed residue presents considerable promise for the elimination of hazardous dyes from

aqueous solutions, serving as a sustainable option for wastewater treatment.

Thus, this study proposes the utilization of fenugreek seed powder (FSP), an abundant agricultural by-product, as a sustainable and low-cost biosorbent for the removal of crystal violet (CV) dye from aqueous solutions. The naturally porous structure and physicochemical properties of FSP enhance its suitability as a biosorbent for dye remediation. To maximize the dye removal efficiency, the experimental conditions were optimized using a statistical Box-Behnken design (BBD), focusing on key parameters such as FSP dosage, contact time, and solution pH. The BBD approach facilitates the simultaneous evaluation of multiple variables to identify optimal conditions for CV removal using FSP. The structural and surface properties of the FSP biosorbent were thoroughly characterized by X-ray diffraction (XRD), Fourier transform infrared spectroscopy (FTIR), and scanning electron microscopy coupled with energydispersive X-ray (SEM-EDX) analysis. Furthermore, the potential dye removal mechanism of CV onto the FSP surface was also investigated to better understand the interaction between the biosorbent and dve molecules.

2. Materials and method

2.1. Materials

Fenugreek seeds were purchased as an agricultural by-product from local sources in Shah Alam, Malaysia. Crystal violet dye (CV: $C_{25}H_{30}ClN_3$, MW: 407.98 g/mol, λ_{max} : 585 nm) was acquired from Sigma-Aldrich (USA). Additional chemicals, including NaOH (99% purity), CH₃COOH (>99% purity), NaCl (>99% purity), and HCl, utilized in this investigation were sourced from R&M Chemicals, Malaysia, and employed without additional purification.

2.2. Fenugreek seeds powder (FSP) preparation steps as a biosorbent

FSP was produced through a series of sequential procedures to guarantee its purity and appropriateness as a biosorbent. The seeds were meticulously rinsed with distilled water to eliminate any residual dust, debris, or contaminants. The purified seeds were subsequently sun-dried for two days, followed by oven drying at 100°C for 24 h to guarantee total moisture elimination. Subsequent to drying, the seeds were pulverized utilizing a mechanical grinder to get a fine powder having a consistent particle size of 250 $\mu \rm m$. The produced FSP was kept in an airtight

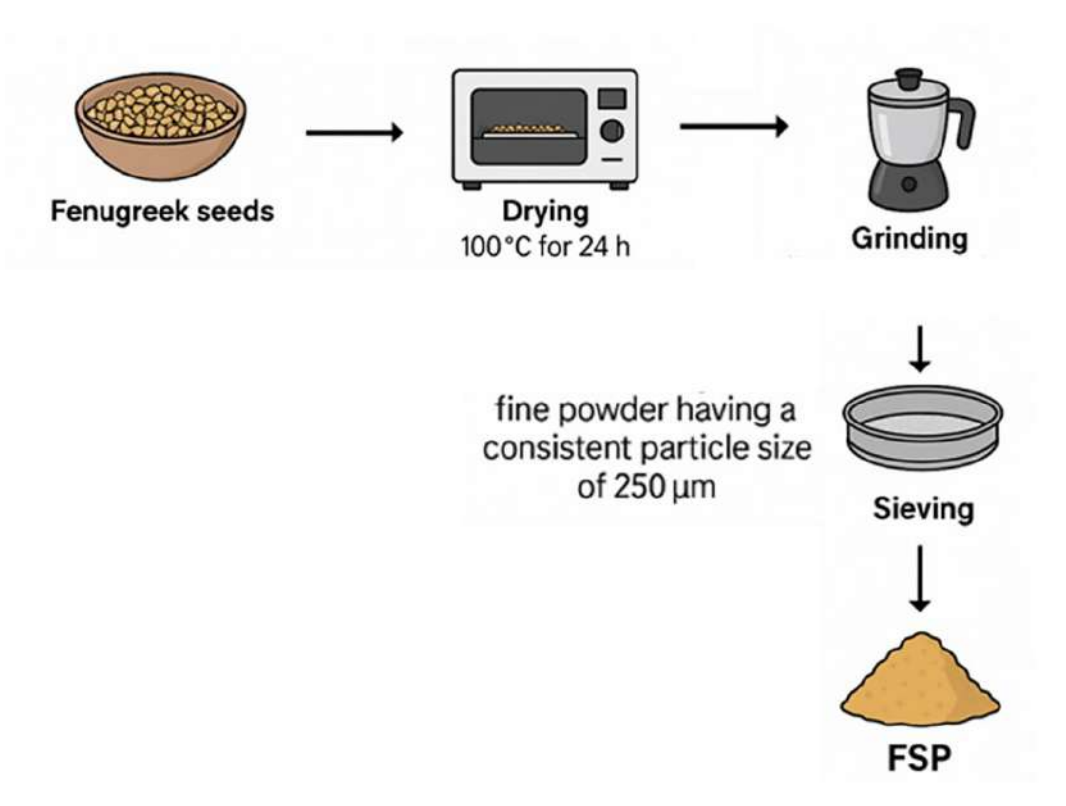


Fig. 1. Preparations steps of FSP.

container to preserve its purity and avert any contamination before subsequent usage (cf. Fig. 1).

2.3. FSP characterization

The crystalline characteristics of FSP powder was examined using an X-ray diffractometer (XRD, X'Pert PRO, PANalytical). To investigate the functional groups present on the surface of FSP before and after CV dye adsorption, Fourier Transform Infrared (FTIR) spectroscopy (Perkin-Elmer, Spectrum RX1) was employed across the spectral range of 4000–450 cm⁻¹. The elemental composition and surface morphology were evaluated through Scanning Electron Microscopy (SEM) coupled with Energy-Dispersive X-ray (EDX) analysis. Additionally, the point of zero charge (pH_{pzc}) of the FSP was determined to explore the surface charge behavior of the biosorbent.

2.4. Experimental design

The RSM-BBD approach was utilized to optimize the biosorption process of CV dye with FSP while reducing the number of experimental trials needed. The Box-Behnken design (BBD) model was utilized to examine the influence of three independent factors on CV removal: FSP dose, solution pH, and contact

Table 1. Codes and actual variables and their levels in BBD.

A FSP (g/100 mL) 0.02 0.06 0.1 B pH 4 7 10 C Time (min) 5 32.5 60	Codes	Variables	Level 1 (-1)	Level 2 (0)	Level 3 (+1)
- F	A	FSP (g/100 mL)	0.02	0.06	0.1
C Time (min) 5 32.5 60	B	pH	4	7	10
	C	Time (min)	5	32.5	60

time. Optimization and statistical analysis were conducted with Design Expert 13.0 software (Stat-Ease, USA). The independent variables, together with their respective ranges and values utilized for CV dye removal by FSP, are presented in Table 1. Table 2 presents the BBD matrix, which comprises 17 experimental runs and their associated responses (CV removal %). A quadratic polynomial model was employed to assess the impact of biosorption factors on the removal efficiency of CV dye, as delineated by Eq. (1):

$$Y = \beta_0 + \sum \beta_i X_i + \sum \beta_{ii} X_i^2 + \sum \sum \beta_{ij} X_i X_j$$
 (1)

In the above equation, Y signifies the % removal of CV dye, X_i and X_j represent the independent variables (FSP dose, pH, and contact duration), β_0 is the constant term, and β_i , β_{ii} , and β_{ij} refer to the linear, quadratic, and interaction coefficients, respectively. The correlation between biosorption parameters and CV dye removal may be elucidated by examining the coefficients derived from fitting

Table 2.	The	3-variables	BBD	matrix	and	experimental	data for
removal of CV by FSP biosorbent.							

Run	A: FSP dose (g/100 mL)	В: рН	C: Time (min)	CV removal (%)
1	0.02	4	32.5	38.4
2	0.1	4	32.5	77.2
3	0.02	10	32.5	79.3
4	0.1	10	32.5	85.5
5	0.02	7	5	61.9
6	0.1	7	5	83.2
7	0.02	7	60	69.7
8	0.1	7	60	91.8
9	0.06	4	5	59.7
10	0.06	10	5	86.2
11	0.06	4	60	70.6
12	0.06	10	60	88.5
13	0.06	7	32.5	82.7
14	0.06	7	32.5	84.9
15	0.06	7	32.5	86.1
16	0.06	7	32.5	84.1
17	0.06	7	32.5	86.3

the experimental data to the regression model. The BBD-RSM methodology enables the determination of optimal operational parameters for enhancing CV dye elimination while minimizing the necessary experimental trials.

The biosorption tests were performed in 250 mL Erlenmeyer flasks, each containing 100 mL of CV dye solution and the specified quantity of FSP according to the BBD matrix (Table 2). The flasks were stirred in a thermostatic water bath shaker at 100 rpm for the appropriate contact time. Following the biosorption process, the FSP biosorbent was separated from the solution using a 0.45 μ m syringe filter. The remaining concentration of CV dye in the filtrate was measured with a UV-Vis spectrophotometer (HACH DR 3900) at 585 nm. The percentage of CV removal (R%) was calculated according to Eq. (2):

$$R \% = \frac{(C_o - C_e)}{C_o} \times 100$$
 (2)

Where C_0 (mg/L) is the initial concentration of CV dye at time zero, and C_e (mg/L) is the equilibrium concentration of CV dye after biosorption.

3. Results and discussion

3.1. Characterization of FSP

The X-ray diffraction (XRD) pattern of FSP displayed a broad diffraction peak within the range of $2\theta = 20^{\circ}-22^{\circ}$ (cf. Fig. 2), signifying the amorphous or semi-crystalline characteristics of lignocellulosic biomass. This property is mostly found in the disordered parts of biopolymers like cellu-

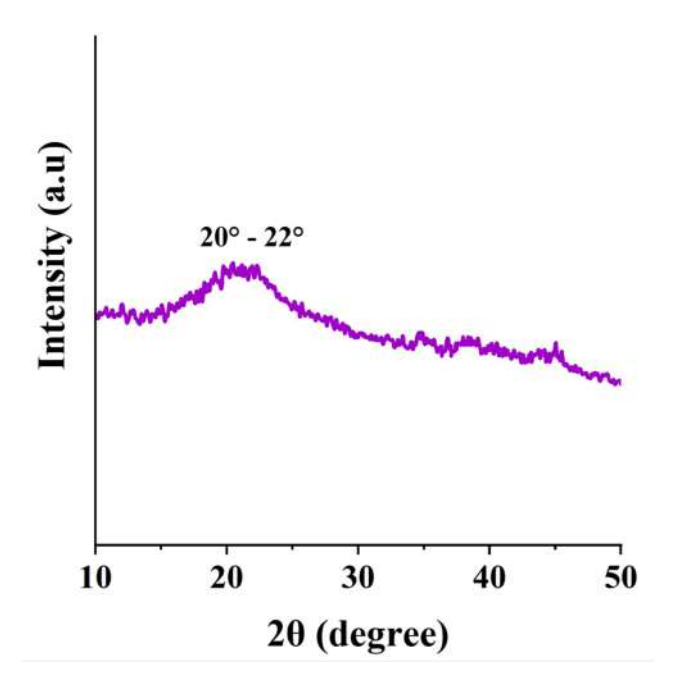


Fig. 2. XRD pattern of FSP adsorbent.

lose, hemicellulose, and starch [17, 30, 31]. The lack of sharp crystalline peaks shows that there are no important inorganic or mineral phases and that the biopolymeric matrix is naturally disordered. Such amorphous traits are often seen in plant-based materials that haven't been treated, and they are linked to a larger surface area and better adsorption properties.

The functional groups present in FSP and their change following CV dye adsorption were analyzed using FTIR. As shown in Fig. 3a and 3b, the spectra display the functional features of FSP before and after dye adsorption. In particular, Fig. 3a shows a prominent absorption band at 3345 cm⁻¹, attributed to vO-H stretching vibrations typically associated with phenolic or alcoholic moieties in lignocellulosic biomass [32, 33]. Additionally, bands observed at 2927 cm⁻¹ (C-H stretching), 1742–1648 cm⁻¹ (C=O stretching), \sim 1545 cm⁻¹ (ν C-C stretching), and 1420 cm⁻¹ (N-H bending) suggest the presence of functional groups such as carboxylic acids, fatty ketones, and amines [34-37]. The peaks observed at 1236 cm⁻¹ and 1065 cm⁻¹ correspond to the C-OH stretching vibrations of amide groups and the C-O/C-O-C stretching vibrations of alcohol, phenol, and ether linkages in polysaccharides, respectively, indicating the presence of proteinaceous and carbohydrate functional groups in FSP [38-40]. FTIR analysis after CV adsorption on FSP (Fig. 3b) reveals alterations in significant peaks, signifying interaction between the dye and surface functional groups. The extensive O-H band (\sim 3345 cm⁻¹) decreases,

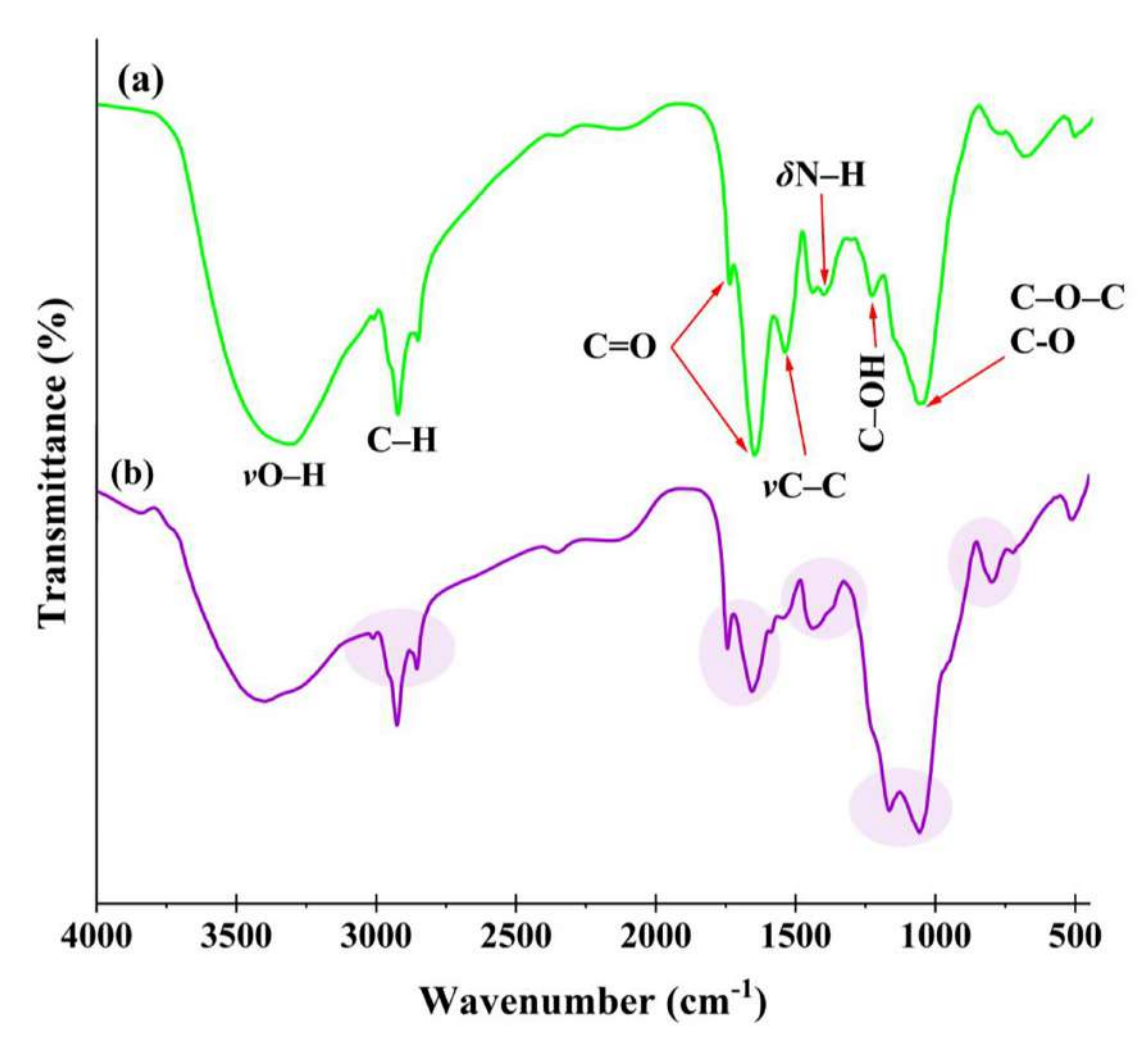


Fig. 3. The FTIR spectra of (a) FSP and (b) FSP after CV biosorption.

indicating hydrogen bonding. Alterations at 1742–1648 cm⁻¹ confirm electrostatic interactions between deprotonated carboxyl groups and the cationic dye [41]. Additionally, alterations at \sim 1065 cm⁻¹ signify C–O and C–O–C stretching, maybe including C–O⁻, suggesting more electrostatic interaction. Further changes in the 1600–1200 cm⁻¹ range corroborate the involvement of carboxylate and phenolic groups in binding [42]. The findings demonstrate that adsorption maybe occurs through electrostatic interactions, hydrogen bonding, and π – π stacking [43].

The surface morphology and elemental distribution of FSP were examined using SEM-EDX before and after the biosorption of CV dye Fig. 4a and 4b. Fig. 4a shows the untreated FSP surface, which appears rough and irregular, with noticeable porosity and scattered agglomerates typical of lignocellulosic biomass. Elemental mapping of the raw sample revealed the dominant presence of carbon (C), oxygen (O), and nitrogen (N). After CV adsorption Fig. 4b,

the FSP surface appeared smoother and more compact, indicating dye deposition and reduced porosity. EDX analysis showed the presence of C, O, and N, along with the appearance of Cl, which is attributed to the crystal violet structure and confirms the dye's presence on the FSP surface.

3.2. Analysis of variance (ANOVA) statistical validation

An ANOVA study was performed to assess the validity of the CV removal model, with the findings displayed in Table 3. The F-model of 126.82, with a p-value under 0.0001, indicates the substantial significance of the employed model. The model's precision and dependability are highlighted by an R^2 value of 0.99, signifying an exceptional fit and accounting for 99% of the variability in the experimental data [44–46]. The modified R^2 of 0.98 aligns closely with the expected R^2 of 0.94, demonstrating that the

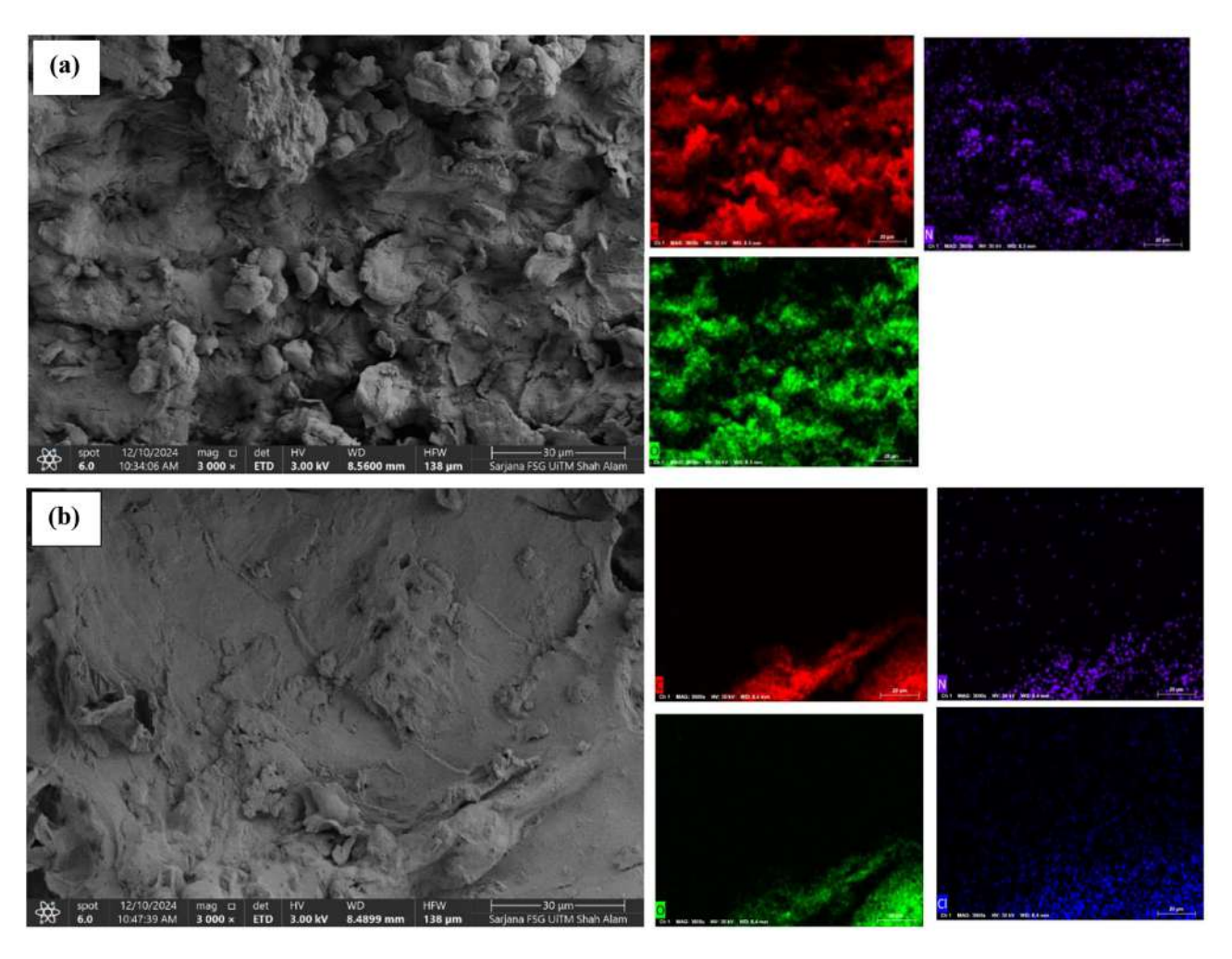


Fig. 4. SEM images at magnification 3kx and EDX results: (a) FSP and (b) FSP+CV dye.

Table 3. Analysis of variance (ANOVA) for CV dye removal onto FSP biosorbent.

Source	Sum of Squares	df	Mean Square	F-value	p-value	Remark
Model	3086.29	9	342.92	126.82	< 0.0001	S*
A-Dose	1067.22	1	1067.22	394.68	< 0.0001	S
B-pH	1095.12	1	1095.12	405.00	< 0.0001	S
C-Time	141.12	1	141.12	52.19	0.0002	S
AB	265.69	1	265.69	98.26	< 0.0001	S
AC	5.76	1	5.76	2.13	0.1878	NS
BC	18.49	1	18.49	6.84	0.0347	S
A^2	186.76	1	186.76	69.07	< 0.0001	S
B^2	273.53	1	273.53	101.16	< 0.0001	S
C^2	1.10	1	1.10	0.4050	0.5448	NS*
Residual	18.93	7	2.70			
Lack of Fit	10.08	3	3.36	1.52	0.3389	NS
Pure Error	8.85	4	2.21			
Cor Total	3105.22	16				
R^2	0.9939		Adjusted R ²	0.9861	Predicted R^2	0.9436
Adeq. Precision	44.3234		C.V. %	2.12		

S*: Significant, NS*: Not significant.

discrepancy is notably smaller than 0.2. This validates the model's resilience, dependability, and significant predictive capacity [47]. The accuracy of 44.3234, much over the threshold of 4, indicates that the model possesses a strong signal-to-noise ratio and is adept at producing reliable predictions. The coefficient variation of 2.12 signifies little deviation from the mean, hence confirming the precision and reliability of the experimental results. The Lack of Fit (LOF) is not significant (p = 0.3389), further validating that the model accurately represents the data without considerable error. All designated statistical criteria validated the suitability of the created model for forecasting CV dye removal [48].

The effectiveness of CV dye removal is influenced by several factors. The p-value, which is less than 0.001, signifies that the impact of these parameters on CV dye removal is statistically significant, as seen in Table 3. A quadratic polynomial demonstrated the statistical correlation between the result and biosorption factors. The correlation between the principal factors affecting CV dye removal is seen in Eq. (3).

CV removal (%) =
$$+84.82 + 11.55A + 11.70B + 4.2C$$

 $-8.15AB + 1.2AC - 2.15BC$
 $-6.66A^2 - 8.06B^2 - 0.5100C^2$
(3)

3.3. Diagnostic plots

Employing graphical tools aids in confirming the accuracy of the model and provides a clear visualization of the residuals' distribution. The distributions of the residual models were evaluated using standard probabilistic diagrams, as seen in Fig. 4. A normal probability plot of residuals is a scatter plot displaying the expected normal distribution percentiles on the x-axis and the residual percentiles on the y-axis. The diagonal line, intersecting the lower and upper quartiles of the theoretical distribution, illustrates the linearity of the connection between theoretical and sample percentiles [21]. Fig. 5a illustrates a linear correlation between theoretical and sample percentiles. The normal probability plot of the residuals demonstrates that the error terms adhere to a normal distribution [49]. The models' effectiveness is demonstrated by the robust linear correlation between the experimental CV removal data and the predicted values, as seen in Fig. 5b. The graph of externally studentized residuals vs run number (Fig. 5c) displayed values ranging from -3.0 to +3.0, signifying little deviation of the model, with the discrepancies adhering to a normal distribution [50]. Fig. 5d displays the Box-Cox plot for power transformation, illustrating the relationship between the natural logarithm of the residual sum of squares [ln(Residual SS)] and various values of the transformation parameter λ . The analysis identified the optimal λ value at 1.0, as indicated by the minimum point on the curve (blue vertical line), corresponding to the lowest ln(Residual SS) value. The 95% confidence interval for λ was estimated to range from approximately 0.43 to 1.8, denoted by the red vertical lines. Since the value $\lambda=1$ lies well within this confidence interval, it can be concluded that the data satisfies the assumptions of normality and constant variance, thereby requiring no transformation [51].

3.4. Response surface plots

A detailed response surface analysis was performed to assess the effects of independent variables and their interactions on CV removal efficiency. The quadratic model facilitated the generation of 3D surface and 2D contour plots, enabling a comprehensive visualization of factor interactions. Key interaction effects and statistical significance are presented in Table 3. Fig. 6a and Fig. 6b illustrates the significant interaction between FSP biosorbent dosage and solution pH on the adsorption capacity of CV dye. The 3D response surface (Fig. 6a) and corresponding contour plot (Fig. 6b) demonstrate that increasing both adsorbent dosage and pH enhances dye removal efficiency. This improvement is attributed to the greater availability of active binding sites at higher adsorbent dosages and the electrostatic attraction between the negatively charged FSP surface and the cationic CV dye at elevated pH levels [17]. As shown in Fig. 6e, the point of zero charge (pHpzc) of FSP was determined to be 6.1, indicating that at pH values above this threshold, the FSP surface becomes increasingly negative. This facilitates stronger electrostatic interactions with CV, thereby enhancing adsorption, as further supported by the adsorption mechanism described in Eq. (4):

$$FSP + O^{-} + CV^{+} \rightleftharpoons FSP + O^{-} \dots CV^{+} \tag{4}$$

Moreover, Fig. 6c and 6d show how solution pH and contact time interact to remove CV. As contact time increased from 5 to 60 minutes, a noticeable increase in removal efficiency was noted at a fixed FSP biosorbent dosage of 0.1 g/100 mL. The longer time frame for dye molecules to diffuse into the internal porous structure of FSP and interact with its active adsorption sites is responsible for this improvement [52]. The removal efficiency increased even more at pH values higher than 7, as the surface of FSP

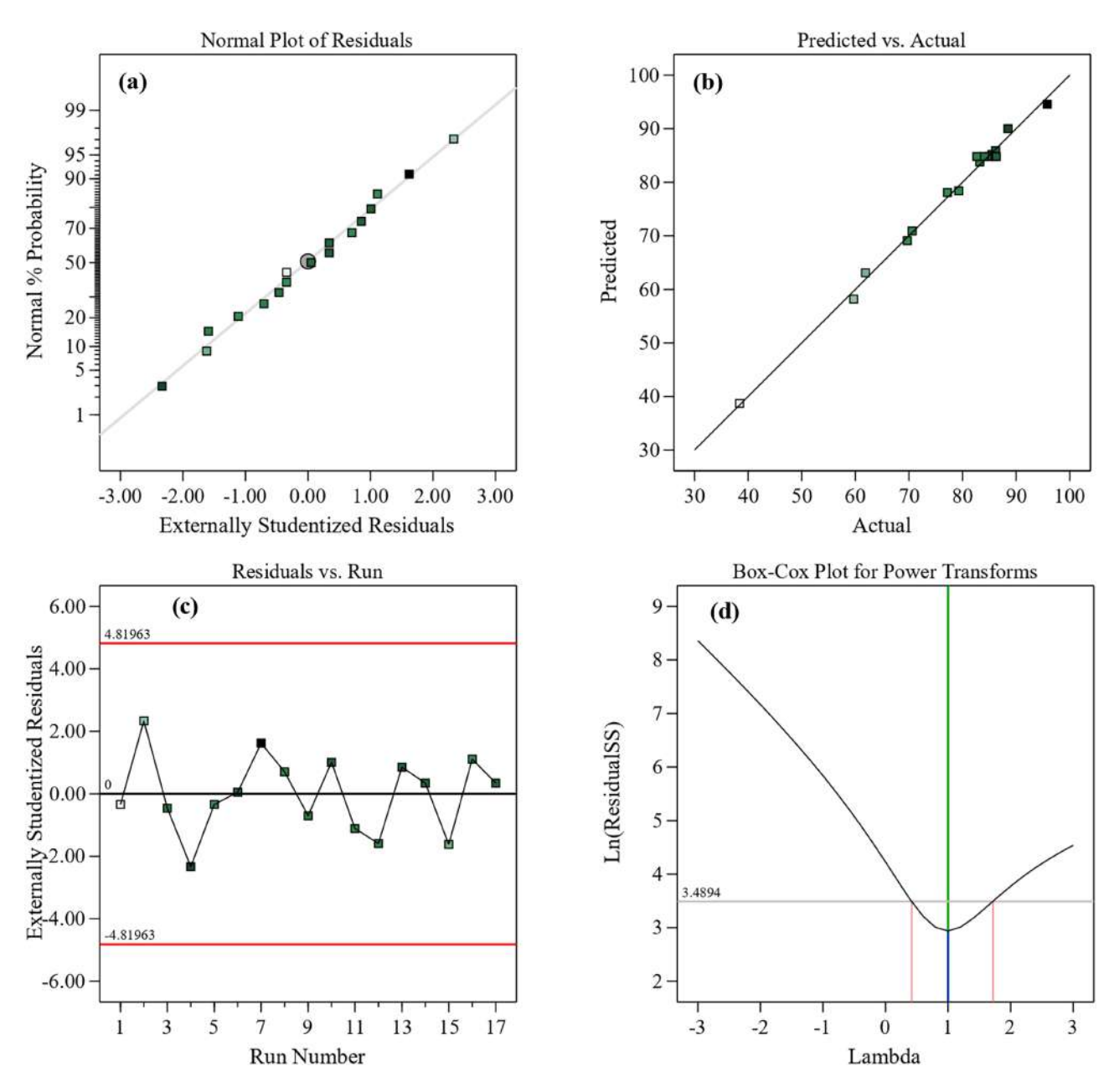


Fig. 5. (a) Normal probability plot of residuals (b) the plot of the relationship between the predicted and actual values (c) residual vs run number (d) Box-Cox plot for CV removal by FSP.

becomes more negatively charged, favoring electrostatic interactions with the cationic dye [53]. These results highlight how crucial pH and contact time are for optimizing CV adsorption because they both affect the biosorbent's surface charge properties and active site accessibility.

4. Biosorption mechanism

The findings of this study demonstrate that the biosorption of CV dye onto FSP biosorbent transpires through a synergistic interaction of various mechanisms, including hydrogen bonding, electrostatic interactions, $\pi - \pi$ stacking, and pore-filling effects, as depicted in Fig. 7. One of the key mechanisms in the biosorption of CV onto FSP is electrostatic attraction, which is primarily caused by the interaction of positively charged dye molecules with negatively charged functional groups on the surface of FSP. The deprotonation of oxygen-containing moieties, such as hydroxyl (–OH) and carbonyl (C=O) groups, causes the negative surface charge. These moieties become more important at solution pH levels higher than the material's point of zero charge (pH_{pzc}). Because of these conditions, the FSP surface has a higher anionic

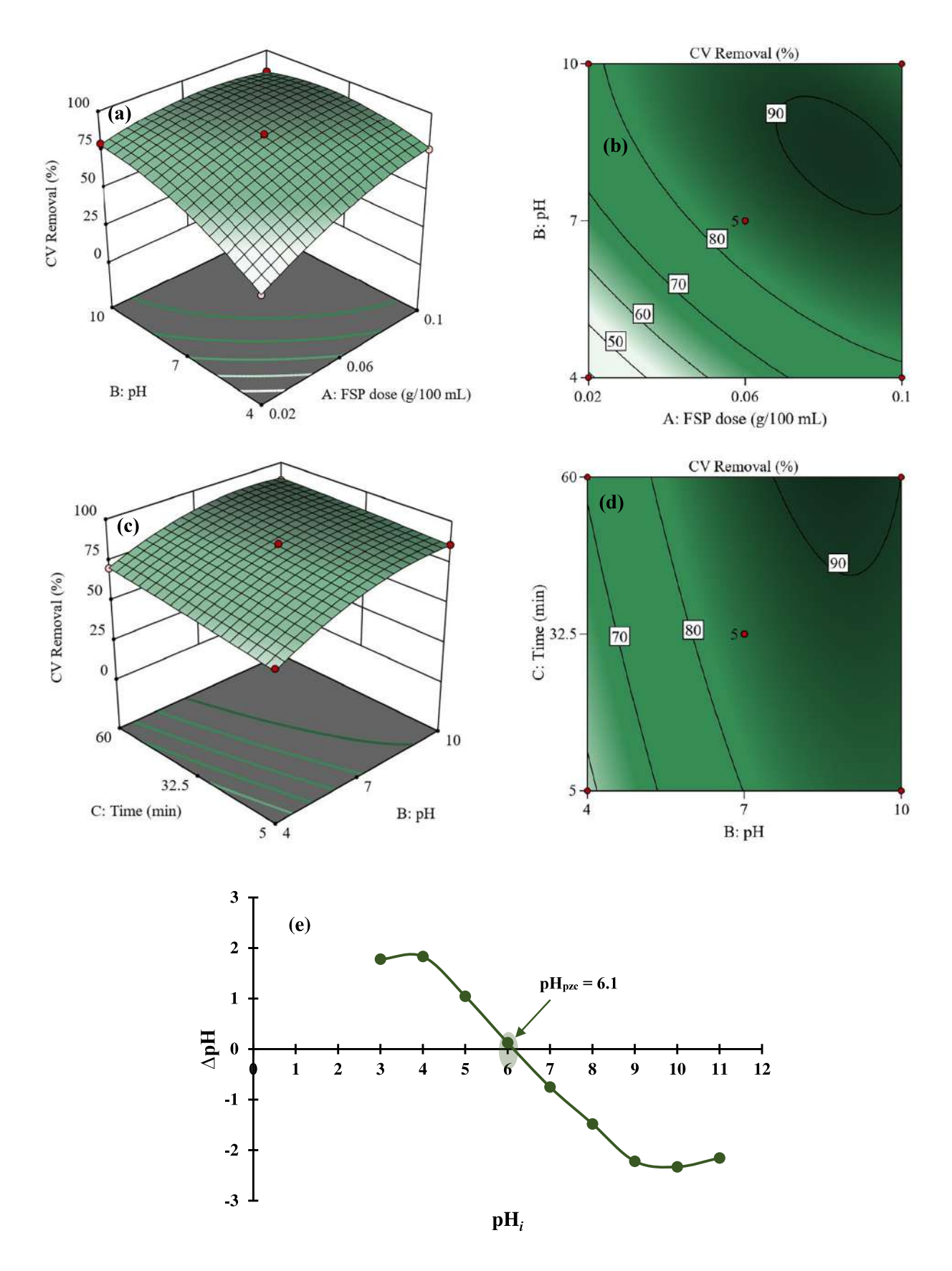


Fig. 6. 3D and 2D response surface plots of significant interactions of (a-b) AB (FSP dose \times pH), and (c-d) BC (pH vs Time) in the CV dye removal, and (e) pH_{pzc} of FSP biosorbent.

Fig. 7. Illustration of the possible interaction between FSP biosorbent and CV dye including electrostatic forces, hydrogen bonding, pore filling, and $\pi - \pi$ interactions. Note that the carboxyl (-COOH) groups are shown in their nonionzed form but would exist in their ionized forms at pH values above the pKa for these groups.

character, which encourages electrostatic interaction with cationic dye species. The pH-dependence of the biosorption process is highlighted by the fact that the interaction is affected by the ionization levels of the dye molecules as well as the functional groups of the biosorbent [54, 55]. Along with electrostatic interactions, hydrogen bonding is a very important part of how CV adsorbs onto FSP. The hydrogen atoms in functional groups on the surface, like -OH and -COOH, make hydrogen bonds with the nitrogen atoms in the CV dye molecules. These specific interactions not only help the adsorption process, but they also help dye molecules stick better to the biosorbent surface [56, 57]. A further significant mechanism that CV adsorbs to FSP is through π – π stacking. This happens when the

conjugated π -electron systems of the aromatic rings in both the biosorbent matrix and the dye molecules interact with each other. These non-covalent $\pi - \pi$ interactions make FSP and CV stickier to each other, especially when the aromatic domains are more likely to line up in a flat way. The porous structure of FSP also allows for pore-filling mechanisms, which means that CV molecules are physically trapped inside the biosorbent's internal cavities and mesoporous channels. This physical confinement also helps the system's overall adsorption capacity and retention efficiency [58]. The intricacy of the adsorption process is further corroborated by FTIR and SEM-EDX investigations, which demonstrate distinct spectrum shifts and alterations in surface morphology after CV uptake. These data validate the

active participation of surface functional groups and the structural alteration of FSP upon contact with dye. The findings together illustrate the efficacy and adaptability of FSP as a sustainable biosorbent for the removal of cationic dyes.

5. Conclusion

The study effectively proved the usefulness of FSP. a plentiful and sustainable agricultural product, as an efficient biosorbent for the removal of CV dve from aqueous solutions. A comprehensive physicochemical analysis demonstrated the amorphous characteristics and abundance of functional groups in FSP, corroborating its significant adsorption capacity. The adsorption process was methodically refined by Box-Behnken design, resulting in a maximum CV removal efficiency of 91.8% at an FSP dose of 0.1 g/100 mL, pH 7, and 60 min contact time. The statistical analysis confirmed the model's high prediction accuracy ($R^2 =$ 0.99, CV = 2.12%) and underscored the substantial impact of adsorbent dose, pH, and contact duration on dye removal. Mechanistic insights, corroborated by FTIR and SEM-EDX investigations, established that CV adsorption onto FSP transpires via a synergistic interplay of electrostatic interactions, hydrogen bonding, π – π stacking, and pore-filling processes. Future research can expand the application of FSP to other dye classes and complex industrial effluents for deeper characterization and develop fixed-bed column studies to assess large-scale feasibility, thereby further validating FSP as a scalable, cost-effective, and environmentally sustainable solution for wastewater treatment.

Conflict of interest

The authors declare no conflict of interest.

Ethical approval

Not applicable.

Data availability

The authors confirm that the data supporting the findings of this study are available within the article [and/or] its supplementary materials.

Funding

The authors declare that no funds, grants, or other support were received during the preparation of this manuscript.

Author contributions

All authors contributed equally to the conception and design of the study.

References

- Periyasamy AP. Textile dyes in wastewater and its impact on human and environment: Focus on bioremediation. Water Air Soil Pollut. 2025;236(9):1–39.
- Murthy GN, Sahu UK. Methylene blue dye removal from aqueous solution using activated carbon prepared from corn cob stem: kinetics, isotherms and mechanism studies. AUIQ Complement Biol Syst. 2025;2(1):35–48.
- Katheresan V, Kansedo J, Lau SY. Efficiency of various recent wastewater dye removal methods: A review. *J Environ Chem Eng.* 2018;6(4):4676–4697.
- Shabna S, Singh CJC, Dhas SDSJ, Jeyakumar SC, Biju CS. An overview of prominent factors influencing the photocatalytic degradation of cationic crystal violet dye employing diverse nanostructured materials. *J Chem Technol Biotechnol*. 2024;99(5):1027–1055.
- Shamsudin NA, Omar Q, Ismail I, Hassan NA, Rahim SA, Dzulkafli NF, Wu R, Yong SK. Oil palm fronds activated carbon via microwave-assisted H3PO4 activation: Box-Behnken optimization for crystal violet dye removal. *AUIQ Complement Biol Sys.* 2024;1(1):77–88.
- Negi A. Environmental impact of textile materials: Challenges in fiber-dye chemistry and implication of microbial biodegradation. *Polymers (Basel)*. 2025;17(7):871.
- 7. Periyasamy AP. Recent advances in the remediation of textile-dye-containing wastewater: Prioritizing human health and sustainable wastewater treatment. *Sustainability*. 2024;16(2):495.
- Mani S, Bharagava RN. Exposure to crystal violet, its toxic, genotoxic and carcinogenic effects on environment and its degradation and detoxification for environmental safety. Rev Environ Contam Toxicol. 2016;237:71–104.
- Chwastowski J, Staroń P, Pieta E, Paluszkiewicz C. Bioremediation of crystal violet by organic matter and assessment of antimicrobial properties of the obtained product. Sustainability. 2022;15(1):67.
- Al-Tohamy R, Ali SS, Li F, Okasha KM, Mahmoud YAG, Elsamahy T, Jiao H, Fu Y, Sun J. A critical review on the treatment of dye-containing wastewater: Ecotoxicological and health concerns of textile dyes and possible remediation approaches for environmental safety. *Ecotoxicol. Environ. Saf.* 2022;231:113160.
- 11. Periyasamy AP. Recent advances in the remediation of textile-dye-containing wastewater: Prioritizing human health and sustainable wastewater treatment. *Sustainability*. 2024;16(2):495.
- Al-Asadi ST, Al-Qaim FF, Al-Saedi HFS, Deyab IF, Kamyab H, Chelliapan S. Adsorption of methylene blue dye from aqueous solution using low-cost adsorbent: Kinetic, isotherm adsorption, and thermodynamic studies. *Environ Monit Assess*. 2023;195(6):676.
- Raja Derisa RR, Awang HF, Hakim Azman M, Rashid I., Hapiz A, Wu R, Reghioua A, Yaseen ZM, Wilson LD. Thermal carbonization of biomass wood dust and algae wastes via microwave-assisted H 3 PO 4: Desirability function and statistical optimization. AUIQ Complement Biol Sys. 2025;2(1):60– 76.

- Al-Qaisi SSA, Raisi A, Alsalhy QF. Novel fabrication techniques for HKUST-1 adsorptive nanocomposite membrane for heavy metals removal from wastewater. Sci Rep. 2025;15(1):14636.
- Dong G, Chen B, Liu B, Hounjet LJ, Cao Y, Stoyanov SR, Yang M, Zhang B. Advanced oxidation processes in microreactors for water and wastewater treatment: Development, challenges, and opportunities. Water Res. 2022;211:118047.
- Mohamed Noor MH, Wong S, Ngadi N, Mohammed Inuwa I, Opotu LA. Assessing the effectiveness of magnetic nanoparticles coagulation/flocculation in water treatment: a systematic literature review. *Int J Environ Sci Technol.* 2022;19(7):6935– 6956
- Agha HM, Jawad AH, Wilson LD, ALOthman ZA. Mild sulfonation process of food grade algae for removal of methyl violet and methylene blue toxic dyes: Statistical modelling and desirability function optimization. *Algal Res.* 2025;89:104040.
- Merah M, Boudoukha C, Avalos Ramirez A, Haroun MF, Maane S. High biosorption of cationic dye onto a novel material based on paper mill sludge. Sci Rep. 2023;13(1):15926.
- Yaashikaa PR, Kumar PS, Saravanan A, Vo DVN. Advances in biosorbents for removal of environmental pollutants: A review on pretreatment, removal mechanism and future outlook. *J Hazard Mater.* 2021;420:126596.
- Stephen DP, Palanisamy SB. Advances in biopolymer composites and biomaterials for the removal of emerging contaminants. *Phys Sci Rev.* 2023;8(8):1789–1809.
- Jawad AH, Deris RRR, Agha HM, Hapiz A, Wu R, ALOthman ZA. Olive (*Olea europaea*) stone powder as a sustainable biosorbent for methyl violet 2B dye removal: multivariable optimization with desirability functions. *Biomass Convers Biorefin.* 2025:1–14.
- Elella MHA, Sabaa MW, Abd ElHafeez E, Mohamed RR. Crystal violet dye removal using crosslinked grafted xanthan gum. Int J Biol Macromol. 2019;137:1086–1101.
- Agha HM, Jawad AH, Wilson LD, ALOthman ZA. Adsorptive performance of sustainable biosorbent from *Macadamia integrifoli* shell powder for toxic methylene blue dye removal: Desirability functions and dye uptake mechanism. *Int J Phytoremediation*. 2025:1–16.
- Vera LM, Bermejo D, Uguña MF, Garcia N, Flores M, González E. Fixed bed column modeling of lead (II) and cadmium (II) ions biosorption on sugarcane bagasse. *Environ Eng Res.* 2019;24(1):31–37.
- Syakina AN, Rahmayanti M. Removal of methyl violet from aqueous solutions by green synthesized magnetite nanoparticles with *Parkia speciosa Hassk*. peel extracts. *Chem Data Collect*. 2023;44:101003.
- Djama C, Bouguettoucha A, Chebli D, Amrane A, Tahraoui H, Zhang J, Mouni L. Experimental and theoretical study of methylene blue adsorption on a new raw material, *Cynara scolymus*—A statistical physics assessment. *Sustainability*. 2023;15(13):10364.
- Agha HM, Sidik NJ, Radzun KA, Jawad AH, Mohammed AA.
 The influence of different concentrations of plant hormones in vitro on seeds germination of fenugreek (*Trigonella foenum-graecum*). *J Asian Sci Res.* 2022;12(2):104–113.
- Taqui SN, CS M, Goodarzi MS, Elkotb MA, Khatoon BA, Soudagar MEM, Koki IB, Elfasakhany A, Khalifa AS, Ali MA, Saifullah Z. Sustainable adsorption method for the remediation of crystal violet dye using nutraceutical industrial fenugreek seed spent. *Appl Sci.* 2021;11(16):7635.
- Dhaif-Allah MAH, Taqui SN, Syed UT, Syed AA. Kinetic and isotherm modeling for acid blue 113 dye adsorption onto lowcost nutraceutical industrial fenugreek seed spent. *Appl Water* Sci. 2020;10:1–16.

- Lindi AM, Falah S, Sadeghnezhad M, Ghorbani M. Optimization of fenugreek seed mucilage extraction for the synthesis of a novel bio-nanocomposite for efficient removal of cadmium ions from aqueous environments. *Int J Biol Macromol.* 2024;261:129882.
- 31. Lindi AM, Gorgani L, Mohammadi M, Hamedi S, Darzi GN, Cerruti P, Fattahi E, Moeini A. Fenugreek seed mucilage-based active edible films for extending fresh fruit shelf life: Antimicrobial and physicochemical properties. *Int J Biol Macromol.* 2024;269:132186.
- Akbari S, Abdurahman NH, Fayaz F, Noory V. Iridoids of fenugreek (*Trigonella foenum-graecum* L.) seed extract detected via LC-QTOF-MS analysis. *Future Foods*. 2021;4: 100067
- Abdulqader MA, Suliman MA, Ahmed TA, Wu R, Bobaker A, Tiyasha T, Yassin MA, Al-Areeq N. Conversion of chicken rice waste into char via hydrothermal, pyrolysis, and microwave carbonization processes: a comparative study. *AUIQ Complement Biol Sys.* 2024;1(1):1–9.
- 34. Tsaousis PC, Sarafidou M, Soto Beobide A, Mathioudakis GN, Filippi K, Bartzialis D, Andrikopoulos KS, Giannoulis KD, Danalatos NG, Koutinas AA, Voyiatzis GA. Quantification of plant biomass composition via a single FTIR absorption spectrum supported by reference component extraction/isolation protocols. *Biomass Convers Biorefin.* 2025:1–16.
- Abdel-Gaber AM, Ezzat A, Mohamed ME. Fenugreek seed and cape gooseberry leaf extracts as green corrosion inhibitors for steel in the phosphoric acid industry. Sci Rep. 2022;12(1):22251.
- Tew WY, Ying C, Wujun Z, Baocai L, Yoon TL, Yam MF, Jingying C. Application of FT-IR spectroscopy and chemometric technique for the identification of three different parts of *Camellia nitidissima* and discrimination of its authenticated product. *Front Pharmacol.* 2022;13:931203.
- Samargandi D, Zhang X, Liu F, Tian S. Fourier transform infrared (FT-IR) spectroscopy for discrimination of fenugreek seeds from different producing areas. 2014.
- Rahman MM, Feng X, Zhang H, Yan X, Peng Q, Yu P. Using vibrational ATR-FTIR spectroscopy with chemometrics to reveal faba CHO molecular spectral profile and CHO nutritional features in ruminant systems. Spectrochim Acta A Mol Biomol Spectrosc. 2019;214:269–276.
- Thombare N, Mahto A, Singh D, Chowdhury AR, Ansari MF. Comparative FTIR characterization of various natural gums: a criterion for their identification. *J Polym Environ*. 2023;31(8):3372–3380.
- Balarak D, Abasizadeh H, Yang J-K, Shim MJ, Lee S-M. Biosorption of acid orange 7 (AO7) dye by canola waste: Equilibrium, kinetic and thermodynamics studies. *Desalin Water Treat*. 2020;190:331–339.
- Baheg NM, Abdel-Hakim A, El-Wakil AEAA, Mekewi M, Halim S. Development of novel natural deep eutectic solvent for cellulose nanofibrillation of orange peel via new surface functionalization. ACS Sustain. Chem. Eng. 2023;11(40):14793– 14806.
- Vara D, Jha S, Bisht S, Shahabuddin S, Gaur R, Suhas, Tyagi
 I. Sustainable bio-based adsorbents for simultaneous and efficient removal of hazardous dyes from aqueous solutions. Toxics. 2024;12(4):266.
- Piquet ABM, Martelli MC. Bioadsorbents produced from organic waste for dye removal: A review. Res Soc Dev. 2022:11(3).
- Patel P, Gupta S, Mondal P. Modeling and optimization of process parameters of MB dye adsorption using waste-derived chemically activated biosorbents. *Biomass Convers Biorefin*. 2023;13(15):13461–13480.

- 45. Shukla AK, Alam J, Mallik S, Ruokolainen J, Kesari KK, Alhoshan M. Optimization and prediction of dye adsorption utilising cross-linked chitosan-activated charcoal: response surface methodology and machine learning. *J Mol Liq.* 2024;411:125745.
- 46. Saleh AM, Mahdi HH, Alias AB, Ali OM, Ghani WAWAK, Shihab TA, Hasan SSAS, Ahmed OK, Saleh NM. Application of response surface methodology (RSM) for optimization of hydrogen sulphide adsorption using coconut shell activated carbon xerogel: Effect of adsorption pressure and hydrogen sulphide flowrate. *Ann Chim Sci Matér.* 2024;509.
- Vellaiyan S, Kandasamy M, Nagappan B, Gupta S, Ramalingam K, Devarajan Y. Optimization study for efficient and cleaner production of waste-derived biodiesel through fuel modification and its validation. *Process Integr Optim Sustain*. 2024;8(3):939–952.
- Kaur M, Kumari S, Sharma P. Response surface methodology adhering central composite design for the optimization of Zn(II) adsorption using rice husk nanoadsorbent. *Chem Phys Lett.* 2022;801:139684.
- Frías-Ureña PM, Bárcena-Soto M, Soto V, Chávez K, Orozco-Guareño E, Badillo-Camacho J, Robledo-Ortiz JR, Fernández-Cervantes I, Gómez-Salazar S. CO₂ capture on Prussian blue analogues (PBAs): Modeling equilibrium, kinetics, and isosteric heats of adsorption. ACS Omega. 2025;10(11):11421–11438
- 50. Rahman SNR, Katari O, Pawde DM, Boddeda GSB, Goswami A, Mutheneni SR, Shunmugaperumal T. Application of design of experiments®approach-driven artificial intelligence and machine learning for systematic optimization of reverse phase high performance liquid chromatography method to analyze simultaneously two drugs (cyclosporin A and etodolac) in solution, human plasma, nanocapsules, and emulsions. AAPS PharmSciTech. 2021;22(4):155.

- 51. Agha HM, Musa SA, Hapiz A, Wu R, Al-Essa K, Saleh AM, Reghioua A. Biocomposite adsorbent of grafted chitosan-benzaldehyde/Lactobacillus casei bacteria for removal of Acid Red 88 dye: Box–Behnken design optimization and mechanism approach. AUIQ Complement Biol Syst. 2025;2(1):1–14.
- Haleem A, Shafiq A, Chen S-Q, Nazar M. A comprehensive review on adsorption, photocatalytic and chemical degradation of dyes and nitro-compounds over different kinds of porous and composite materials. *Molecules*. 2023;28(3):1081.
- 53. Onuk EB, Isik B. Adsorptive removal of toxic methylene blue and crystal violet dyes from aqueous solutions using *Prunus spinosa*: Isotherm, kinetic, thermodynamic, and error analysis. *Biomass Convers Biorefin.* 2025:1–18.
- Agha HM, Allaq A, Jawad AH, Aazmi S, ALOthman ZA, Wilson LD. Immobilization of *Bacillus subtilis* bacteria into biohybrid crosslinked chitosan-glutaraldehyde for Acid Red 88 dye removal: Box–Behnken design optimization and mechanism study. *J Inorg Organomet Polym Mater.* 2024. doi:10.1007/s10904-024-03264-4.
- Rápó E, Tonk S. Factors affecting synthetic dye adsorption; desorption studies: A review of results from the last five years (2017–2021). *Molecules*. 2021;26(17):5419.
- Nath J, Kumar S, Kumar V. Fabrication and characterization of fenugreek-g-poly(acrylic acid) hydrogel for effective adsorption of crystal violet dye. *Adsorption*. 2025;31(1):4.
- 57. Patel P, Gupta S, Mondal, P. Modeling and optimization of process parameters of MB dye adsorption using wastederived chemically activated biosorbents. *Biomass Convers Bioref.* 2023;13(15):13461-13480.
- Al-Gethami W, Qamar MA, Shariq M, Alaghaz ANMA, Farhan A, Areshi AA, Alnasir, MH. Emerging environmentally friendly bio-based nanocomposites for the efficient removal of dyes and micropollutants from wastewater by adsorption: A comprehensive review. RSC Adv. 2024;14(4):2804–2834.